

RESEARCH ARTICLE

The dual role of a highly structured RNA (the S fragment) in the replication of foot-and-mouth disease virus

Joseph C. Ward¹  | Lidia Lasecka-Dykes²  | Samuel J. Dobson¹  | Sarah Gold²  |
Natalie J. Kingston¹  | Morgan R. Herod¹  | Donald P. King²  |
Tobias J. Tuthill²  | David J. Rowlands¹  | Nicola J. Stonehouse¹ 

¹School of Molecular and Cellular Biology, Faculty of Biological Sciences and Astbury Centre for Structural Molecular Biology, University of Leeds, Leeds, UK

²The Pirbright Institute, Surrey, UK

Correspondence

David J. Rowlands and Nicola J. Stonehouse, School of Molecular and Cellular Biology, Faculty of Biological Sciences and Astbury Centre for Structural Molecular Biology, University of Leeds, Leeds, UK.
Email: d.j.rowlands@leeds.ac.uk and n.j.stonehouse@leeds.ac.uk

Funding information

UKRI | Biotechnology and Biological Sciences Research Council (BBSRC), Grant/Award Number: BB/K003801/1, BBS/E/I/00007035, BBS/E/I/00007036 and BBS/E/I/00007037; Department for Environment, Food and Rural Affairs, UK Government (Defra), Grant/Award Number: SE2945

Abstract

Secondary and tertiary RNA structures play key roles in genome replication of single-stranded positive sense RNA viruses. Complex, functional structures are particularly abundant in the untranslated regions of picornaviruses, where they are involved in initiation of translation, priming of new strand synthesis and genome circularization. The 5' UTR of foot-and-mouth disease virus (FMDV) is predicted to include a c. 360 nucleotide-long stem-loop, termed the short (S) fragment. This structure is highly conserved and essential for viral replication, but the precise function(s) are unclear. Here, we used selective 2' hydroxyl acetylation analyzed by primer extension (SHAPE) to experimentally determine aspects of the structure, alongside comparative genomic analyses to confirm structure conservation from a wide range of field isolates. To examine its role in virus replication in cell culture, we introduced a series of deletions to the distal and proximal regions of the stem-loop. These truncations affected genome replication in a size-dependent and, in some cases, host cell-dependent manner. Furthermore, during the passage of viruses incorporating the largest tolerated deletion from the proximal region of the S fragment stem-loop, an additional mutation was selected in the viral RNA-dependent RNA polymerase, 3D^{pol}. These data suggest that the S fragment and 3D^{pol} interact in the formation of the FMDV replication complex.

KEYWORDS

3D^{pol}, 5' UTR, FMDV, picornavirus replication, S fragment, SHAPE

Abbreviations: ATCC, American Type Culture Collection; ATP, adenosine triphosphate; BBSRC, Biotechnology and Biological Sciences Research Council; BHK, baby hamster kidney; BLAST, Basic Local Alignment Search Tool; BWA, Burrows-Wheeler Aligner; CPE, cytopathic effect; *cre*, cis-acting replicative element; CTP, cytidine triphosphate; Defra, Department for the Environment, Food and Rural Affairs; DMEM, Dulbecco's Modified Eagle Medium; DMSO, dimethyl sulfoxide; DNA, deoxyribonucleic acid; FCS, fetal calf serum; FMD, foot-and-mouth disease; FMDV, foot-and-mouth disease virus; GTP, guanosine triphosphate; HTS, high throughput sequencing; IGV, Integrative Genomics Viewer; IRES, internal ribosome entry site; MDBK, Madin-Darby bovine kidney; MOPS, 3-(*N*-morpholino) propanesulfonic acid; NMIA, *N*-Methylisatoic anhydride; NTP, ribonucleotide triphosphate; O1K, O1 Kaufbeuren; PV, poliovirus; RdRp, RNA-dependent RNA polymerase; RNA, ribonucleic acid; S fragment, short fragment; SAT, Southern African Territories; SEM, standard error of the mean; SHAPE, selective 2'-hydroxyl acylation analyzed by primer extension; SRA, Sequence Read Archive; TE, Tris-EDTA; UTP, uridine triphosphate; UTR, untranslated region; WT, wild type.

This is an open access article under the terms of the [Creative Commons Attribution](https://creativecommons.org/licenses/by/4.0/) License, which permits use, distribution and reproduction in any medium, provided the original work is properly cited.

© 2024 The Author(s). *The FASEB Journal* published by Wiley Periodicals LLC on behalf of Federation of American Societies for Experimental Biology.

1 | INTRODUCTION

The genomes of single-stranded positive sense RNA viruses include both coding and regulatory regions. Picornaviruses are amongst the smallest, with genomes approximately 7.5–8 kb in length. Typically, the genome comprises a major single open reading frame flanked by 5' and 3' untranslated regions (UTRs); however, additional small open reading frames have been identified in some cardioviruses and enteroviruses.^{1,2} The large 5' UTRs present in most picornaviruses range from ~800 to ~1300 nucleotides and have been predicted in silico by energy minimization algorithms to comprise several distinct highly structured domains.^{3–10} Some of these RNA structures are common for all picornaviruses and have been well characterized, for example, an internal ribosome entry site (IRES) responsible for the initiation of translation, which comprises ~450 nucleotides for most picornaviruses (although smaller IRES elements resembling those found in some flaviviruses were also found).^{3,11,12} The number and organization of these structural domains vary among picornaviruses. For example, a small stem-loop, the *cis*-active replicative element (*cre*), which is essential for replication, is found in the 5' UTR of aphthoviruses, but within the coding region in enteroviruses.^{4–6} All picornavirus genomes include a structured domain at the 5' end, although the size, conformation, and sequence vary in viruses from different genera. Enterovirus 5' UTRs terminate in a ~80 nucleotide cloverleaf structure, while in some other picornaviruses, the 5' end forms an extended stem-loop.^{7,8,13} The size of this stem-loop varies markedly; 40 nucleotides in hepatoviruses and ~80 nucleotides in cardioviruses, whereas the largest (~360 nucleotides) is present in the aphthoviruses.¹⁴ The functions of some of these RNA structures remain unknown.

Here, we focus on the long 5' terminal stem-loop (termed S fragment) of foot-and-mouth disease virus (FMDV), an aphthovirus which infects cloven-hoofed animals. This is the causative agent of foot-and-mouth disease (FMD), a highly contagious and economically important infection posing a constant threat to the global livestock industry. In endemic countries, FMD is controlled by vaccination and by movement restrictions, while movement restrictions and slaughter have been used when outbreaks occurred in non-endemic countries.¹⁵ Control by vaccination is complicated by high antigenic variability and the occurrence of asymptomatic carrier animals.^{16–18} FMDV has an 8.5 kb RNA genome organized into L, P1-2A, P2 and P3 coding regions, flanked by the 5' UTR described above and a short 3' UTR. L is a protease responsible for separating itself from the polyprotein and cleaving key cellular proteins, P1 encodes the structural (capsid) proteins, while P2 and P3 encode non-structural proteins involved

in genome replication. The latter include the RNA-dependent RNA polymerase (RdRp, also termed 3D^{pol}) and the protease 3C^{pro}, alongside less well-characterized proteins including 2C, a potential helicase.^{19–21} At approximately 1.3 kb, the 5' UTR of FMDV is ~1/7th of the entire genome and is the longest 5' UTR within the picornavirus family.⁸ Its sequence comprises at least five structurally and functionally distinct domains. The S fragment stem-loop (c. 360 nucleotides) is located at the 5' terminus and is followed by a long poly-C-tract of variable length (about 70–250 nucleotides), 2–4 tandem repeated sequences predicted to form pseudoknots, the small stem-loop *cre* involved in uridylation of the replication primer peptide VPg and finally the IRES element responsible for protein translation initiation.²² The functions of several of these domains are poorly understood,^{23,24} although we have recently described the importance of a sequence in the pseudoknot region for virus assembly.⁹

While the S fragment is known to be essential for replication, its precise function remains unclear. The secondary structure of the S fragment appears to be conserved, although its sequence and length varies between different clades of FMDV.^{8,10} Truncated S fragments have been observed for some field isolates, but these retain the long stem-loop structure.⁸ It has been reported that while distal portions of this stem-loop structure are not essential for genome replication, they play a role in the modulation of host-cell innate immune responses.^{25,26} The 5' end of poliovirus (PV) RNA also terminates in a highly structured region, called the cloverleaf, which is involved in the switch from protein translation to RNA replication, in addition to recruiting host and viral proteins which contribute to RNA circularization during genome replication.^{7,27} It is possible that the S fragment in FMDV has similar functions; it is known to interact with the 3' UTR, suggesting a role in genome circularization.²⁸

We used selective-2' hydroxyl acylation analyzed by primer extension (SHAPE) to provide direct evidence to complement comparative bioinformatic analyses and in silico predictions of the structure of the S fragment. We confirm that substantial deletions can be made to the distal region of the S fragment stem-loop without seriously compromising in vitro replication, although host cell differences were observed. We also show that proximal deletions are less well tolerated, which correlates with our observation that the proximal part of the S fragment shows higher conservation of nucleotide pairings. Furthermore, viruses reconstructed to include the maximal viable proximal deletion can, during sequential passages, select a compensatory mutation in the 3D^{pol}. This mutation is located in a highly conserved position known to interact with template RNA and enhanced replication of a mutant replicon carrying this proximal S fragment deletion.

2 | MATERIALS AND METHODS

2.1 | Cell lines

Baby hamster kidney (BHK)-21 and Madin-Darby bovine kidney (MDBK) cells were obtained from the American Type Culture Collection (ATCC) (LGC Standard) and maintained in Dulbecco's modified Eagle's Medium (DMEM) with glutamine (Sigma-Aldrich) supplemented with 10% fetal calf serum (FCS), 50 U/mL penicillin and 50 µg/mL streptomycin as previously described.²⁹

2.2 | Plasmid construction

The FMDV ptGFP replicon plasmids along with the equivalent 3D^{pol} knock-out controls (3D^{pol}-GNN) have already been described.^{30,31}

A variant of the ptGFP replicon was produced to allow for easy mutagenesis of the S-fragment. An *EagI* site was introduced at each end of the S-fragment by PCR mutagenesis, altering the wild-type sequence from AAAGGGGGCATTAA to AAACGGCCGATTAA at the 5' end and GCGCCCGCTTTT to GCGCGCCGTTTT at the 3' end. S fragment sequences containing deletions were chemically synthesized (Thermo Fisher Scientific) and inserted into the replicon vector using complementary *EagI* sites.

Mutation of residue I189L of 3D^{pol} in the ptGFP replicon was achieved by PCR mutagenesis resulting in A7023C substitution.

Primer sequences are provided in [Table S1](#).

2.3 | Protein purification

The I189L mutation was introduced into the His-tagged 3D^{pol} expression clone pET28a-3D, and recombinant protein was expressed and purified as previously described.^{32,33}

2.4 | In vitro transcription

In vitro transcription reactions were performed as described previously.^{34,35} Briefly, 5 µg of replicon plasmid was linearized with *AscI* (NEB), purified by phenol-chloroform extraction, ethanol precipitated, redissolved in RNase-free water, and used in a T7 in vitro transcription reaction. Reactions were incubated at 32°C for 4h, treated with 1.25 units of RQ1 DNase for 30 min at 37°C and RNA recovered using an RNA Clean & Concentrator-25 spin column kit (Zymo Research),

following manufacturer's instructions. All transcripts were quantified by NanoDrop 1000 (Thermo Scientific) and RNA integrity was assessed by 3-(*N*-morpholino) propanesulfonic acid (MOPS) -formaldehyde gel electrophoresis.

2.5 | Replication assays

BHK-21 and MDBK cell based replicon replication assays were performed in 24-well plates with 0.5 µg/cm² of RNA using Lipofectin transfection reagent (Life Technologies) as previously described.³⁵ For every experiment, transfection was performed in duplicate and experiments biologically repeated as indicated. Replicon replication was assessed by live cell imaging using an IncuCyte Zoom Dual color FLR, an automated phase-contrast and fluorescent microscope within a humidifying incubator. At hourly intervals up to a defined end point, images of each well were taken and used to enumerate the ptGFP positive cell count per well, using our established protocols.^{34,35} Data are shown at 8 h post transfection (when maximum replication was observed) on a linear scale.

2.6 | SHAPE analysis

RNA transcripts representing the entire 5' UTR of FMDV (nucleotides 1–1581) were prepared as above. A sample containing 12 pmol of transcribed RNA was heated to 95°C for 2 min before cooling on ice. RNA folding buffer (100 mM HEPES, 66 mM MgCl₂, and 100 mM NaCl) was added to the RNA and incubated at 37°C for 30 min. The folded RNA was treated with 5 mM *N*-methylisatoic anhydride (NMIA) or dimethyl sulfoxide (DMSO) for 50 min at 37°C. The chemically modified RNA was ethanol precipitated and resuspended in 0.5× Tris-EDTA (TE) buffer.

Hex or FAM fluorescent primers were bound to modified RNA by heating the reaction to 85°C for 1 min, 60°C for 10 min, and 35°C for 10 min in a thermocycler. Reverse transcription was continued using Superscript III (Invitrogen) following the manufacturer's protocol with incubation at 52°C for 30 min.

Post-extension, cDNA:RNA hybrids were dissociated by incubation with 4M NaOH at 95°C for 3 min before neutralization with 2M HCl. Extended cDNA was ethanol precipitated and resuspended in deionized formamide (Thermo Fisher Scientific). Sequencing ladders were similarly produced using 6 pmol of RNA with the inclusion of 10 mM ddCTP in the reverse transcription mix and using a differentially labeled fluorescent primer (either Hex or FAM). A sequencing ladder was combined with NMIA or DMSO samples and dispatched on dry ice for

capillary electrophoresis (DNA Sequencing and Services, University of Dundee).⁹

NMIA reactivity was used as constraints for RNA secondary structure prediction of the S fragment using the Vienna RNA probing package and based on the sequence of the replicon used in this study.³⁶

2.7 | Construction of recombinant viruses

Replicons used here are based on plasmid pT7S3 which encodes a full-length infectious copy of FMDV O1 Kaufbeuren (O1K).³⁷ To generate infectious viral genomes the reporter sequence was removed from replicons by digestion with flanking *PsiI* and *XmaI* restriction enzymes and replaced with the corresponding fragment from pT7S3 encoding the capsid proteins. Full-length viral RNA was transcribed using a T7 MEGAscript kit (Thermo Fisher Scientific), DNase treated using TurboDNase (Thermo Fisher Scientific), and purified using a MEGAclear Transcription Clean-Up kit (Thermo Fisher Scientific). RNA quality and concentration were determined by MOPS-formaldehyde denaturing agarose gel electrophoresis and Qubit RNA BR Assay Kit (Thermo Fisher Scientific).

2.8 | Virus recovery

BHK-21 cells were transfected in 25 cm² flasks with 8 μg per flask of infectious clone-derived RNA using TRANSIT transfection reagent (Mirus) as described previously.³⁵ At full cytopathic effect (CPE) or 24 h post-transfection (whichever was earlier), cell lysates were freeze-thawed and clarified by centrifugation. The clarified lysate (1 mL) was blind passaged onto naïve BHK-21 cells and this was repeated for five rounds of passaging.

2.9 | Sequencing of recovered virus

Recovered viruses at passage 3, 4, and 5, were sequenced with an Illumina MiSeq (Illumina) using a modified version of a previously described PCR-free protocol.³⁸ Total cellular RNA was extracted from clarified infected cell lysates using TRIZOL reagent (Thermo Fisher Scientific) and residual genomic DNA was removed using DNA-free DNA removal Kit (Thermo Fisher Scientific) prior to ethanol precipitation. Purified RNA was used in a reverse transcription reaction as previously described and followed by second-strand synthesis.^{38,39} Phenol-chloroform purified cDNA was quantified using a Qubit ds-DNA HS

Assay kit (Thermo Fisher Scientific) and a cDNA library prepared using Nextera XT DNA Sample Preparation Kit (Illumina). Sequencing was carried out on the MiSeq platform using MiSeq Reagent Kit v2 (300 cycles) chemistry (Illumina) and paired-end sequencing. Individual raw fastq files were submitted to Sequence Read Archive (SRA) (accession numbers: SRR29218774-SRR29218779) under BioProject accession number PRJNA1116147.

FastQ files were quality checked using FastQC with poor quality reads filtered using the Sickle algorithm.⁴⁰ Host cell reads were removed using the FastQ Screen algorithm and FMDV reads assembled de novo into contigs using IDBA-UD.⁴¹ Contigs that matched the FMDV library (identified using Basic Local Alignment Search Tool (BLAST)) were assembled into consensus sequences using SeqMan Pro software implemented in the DNA STAR Lasergene 13 package (DNA STAR).⁴² Finally, the filtered fastQ reads were aligned to the de novo constructed consensus sequences using the BWA-MEM algorithm incorporated into Burrows-Wheeler Aligner (BWA), and mutations were visualized using the Integrative Genomics Viewer (IGV).⁴³⁻⁴⁶

2.10 | Cell killing assays

Virus titer was determined by plaque assay on BHK-21 cells as described before.⁴⁷ BHK-21 cells were seeded with 3×10^4 cells/well in 96 well plates and allowed to settle overnight. Cell monolayers were inoculated with each rescued virus at MOI of 0.01 PFU for 1 h, inoculum was removed and 150 μL of fresh DMEM (supplemented with 1% FCS) was added to each well. The appearance of CPE was monitored every hour by live cell microscopy (contrast phase) using the IncuCyte S3 (Sartorius). CPE was observed as rounding of the cells and progress of infection was monitored as a drop in confluency compared to the mock-treated cells (i.e., treatment with uninfected cell lysate). Serial images of cells were analyzed using IncuCyte S3 2018B software.

2.11 | Sym/Sub polymerase activity assays

Sym/Sub RNA with sequence 5' GCAUGGGCCC 3' was synthesized (Sigma Aldrich) and 5' end-labeled using γ -³²P UTP (Perking Elmer) and T4 polynucleotide kinase (NEB) following the manufacturer's protocol. Labeled RNA was purified by ethanol precipitation and resuspended in nuclease-free water.

0.5 μM of end-labeled RNA was incubated in polymerization buffer (30 mM MOPS pH 7.0, 33 mM NaCl, 5 mM

MgAc) and heated to 95°C for 2 min before chilling on ice. 2 μM of recombinant 3D^{pol} was added to the RNA and incubated at 37°C for 10 min to promote annealing. After annealing, 50 μM of rNTP was added to the reaction, the addition of nucleotide varied depending on the experiment. Aliquots were taken periodically, and reactions were stopped by the addition of 2× TBE-urea RNA loading dye (Thermo Fisher Scientific).

Extension products in loading dye were heated to 70°C for 5 min before loading on a 23% denaturing polyacrylamide gel containing 7M urea. Samples were electrophoresed until sufficiently separated. After electrophoresis, gels were fixed for 30 min in a fixative solution and exposed to a phosphor screen.^{48,49}

2.12 | Bioinformatic analyses

Full genome sequences of 118 FMDV isolates, representing all seven serotypes (Table S2), were downloaded from GenBank. The sequences were chosen (based on the region encoding the VP1 protein) to represent the known genomic diversity of FMDV across all seven serotypes. VP1 is the most variable part of the FMDV genome and is frequently used to calculate the phylogenetic relationship of FMDV isolates.^{8,26,50}

The RNA structure of the S fragment was predicted as described before using the RNAalifold program implemented in the ViennaRNA package.^{36,51} For the covariance analysis, also calculated using the RNAalifold program, only those isolates were included which contained a complete sequence at the 5' end of the genome. Data representing covariance were superimposed onto the schematics of the S fragment RNA structure and visualized using the Forna tool implemented in the ViennaRNA Web Services.⁵² The sequence logo representing amino acid conservation within positions 185–194 of the 3D^{pol} was prepared using a WebLogo 3.7.4 server and using 1123 FMDV 3D^{pol} sequences obtained from fmdbase.org (an FMDV sequence database generated by the FAO World Reference Laboratory for FMD at The Pirbright Institute).^{53,54}

2.13 | RNA stability assay

Radiolabelled RNA was made by incubating 1 μg linearized DNA template (described above) with 2 mL 10× RNA polymerase buffer (Invitrogen) and 0.5 μL RNA secure (Invitrogen). Nuclease free water was added to make a total volume of 20 μL and the reaction heated to 60°C for 10 min. Post incubation, 1 μL of 10 mM ATP, CTP and GTP were added alongside 2.4 μL 100 mM UTP, 5 μL 10 mCi/

mL α³²P UTP (Perkin Elmer). Finally, 1 μL RNase out and T7 polymerase were added before incubation at 37°C for 2 h. Reactions were DNase treated with the addition of 1 μL DNase (Promega) before incubation at 37°C for 20 min. Radiolabelled RNA was purified using RNA Clean and Concentrator columns (Zymo Research) before quantification by spectroscopy.

RNA stability was measured by incubation of 4 mg of α³²P UTP labeled RNA in 50 μL untreated rabbit reticulocyte lysate (Promega) and incubated at 30°C. At 0, 20 and 40 min 7 μL samples were removed and added to 150 μL TRIzol (Invitrogen), incubation in TRIzol was allowed to continue for 10 min at room temperature before purification using the Direct-Zol RNA purification kit (Zymo Research). Purified RNA samples were analyzed on an RNA-MOPs gel (described above) before drying using a Bio-Rad Gel dryer. Dried gels were exposed to a phosphor screen and signal measured using a phosphorimager.

2.14 | Statistical analysis

Statistical analysis was conducted using one way ANOVA with Tukey simultaneous tests for differences of means. Error bars represent standard error of the mean (SEM).

3 | RESULTS

3.1 | SHAPE analysis of the S fragment

Based on computational folding, such as mFOLD algorithms, the S fragment is predicted to form a single large hairpin stem-loop comprising approximately 360 nucleotides.¹⁰ Here, we use selective 2' hydroxyl acylation analyzed by primer extension (SHAPE) to further investigate the structure of this part of the FMDV genome. This approach relies on the formation of 2'-O-adducts in single stranded and accessible regions of the RNA, which can then be detected by reverse transcription.

RNA transcripts representing the full FMDV 5' UTR were folded before incubation with NMIA. The modified RNAs were then used in reverse-transcription reactions containing fluorescently end-labeled primers. Reverse transcription is terminated when the enzyme reaches a nucleotide with a NMIA adduct, thus creating a series of cDNA fragments of different lengths. These cDNA fragments were analyzed by capillary gel electrophoresis alongside a sequencing ladder to identify the sites of termination, indicating the locations of unpaired and accessible nucleotides. The proximity of the poly-C-tract to the 3' end of the S fragment limited potential primer binding sites, resulting in unreliable data for the last 60

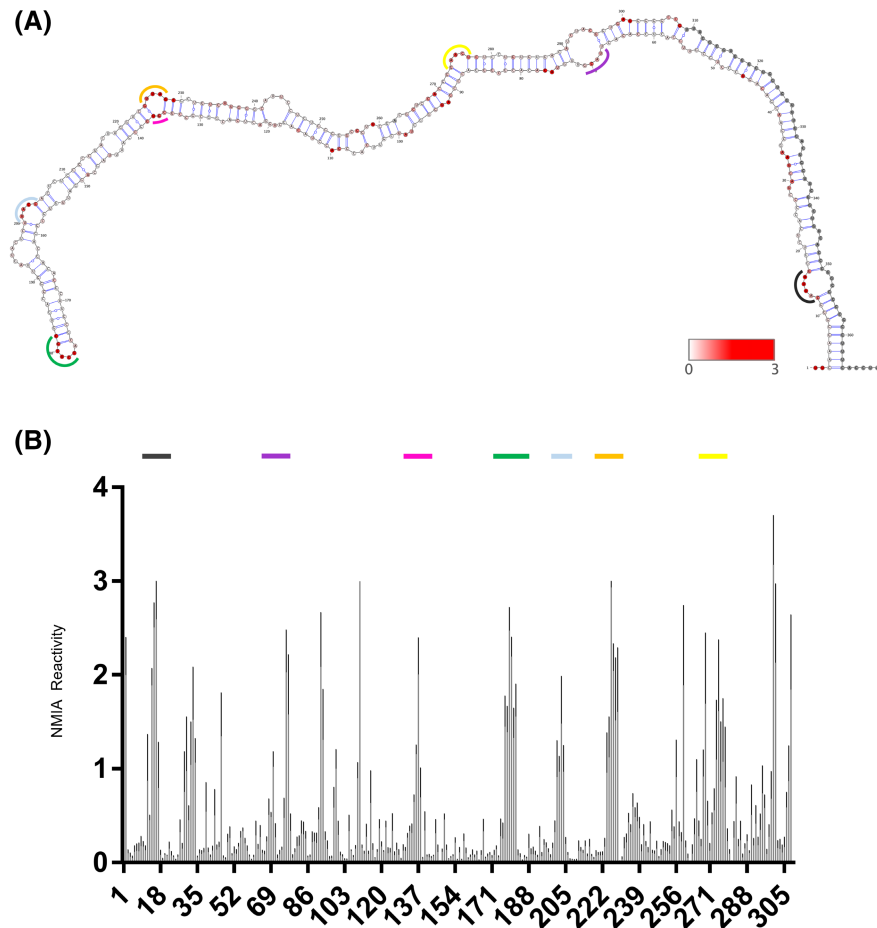


FIGURE 1 SHAPE analysis of the S fragment. (A) Superimposition of SHAPE reactivity on the in silico predicted secondary structure WT S fragment. Secondary structure was predicted using the Vienna RNA probing package and visualized using VARNA. NMIA reactivity is overlaid and represented on a color scale from low (white) to high (red). Nucleotides for which there is no data are represented as gray. Colored regions corresponding to the peaks in NIMIA reactivity are shown for ease of interpretation and localization. (B) Individual nucleotide NMIA reactivity as analyzed by SHAPE reactions and capillary electrophoresis. High reactivity indicates high probability of single-stranded regions, i.e. non base-paired nucleotides. Data were analyzed using QuSHAPE. Corresponding colored regions are shown for some regions across A and B for ease of interpretation and localization of SHAPE data to RNA structure ($n=6$, error bars represent SEM).

nucleotides of the S fragment which were excluded from the analysis (shown in gray in Figure 1A). The rest of the S fragment was well covered and the SHAPE reactivities from 6 independent experiments were used to complement the mFOLD algorithm analyses to generate a structural prediction of this region (Figure 1).

In general, the SHAPE mapping data fitted well with the in silico predictions with the most reactive residues coinciding with bulges within the predominately double stranded stem-loop structure (Figure 1A). The locations of reactive residues can be seen in the NMIA reactivity graph, where groups of nucleotides within bulges showed high reactivity (Figure 1B). However, some predicted bulges showed little NMIA reactivity, suggesting steric hindrance possibly due to higher order tertiary structure. Similarly, some predicted base-paired nucleotides were NMIA reactive. These mostly occurred at the tops and bottom of bulges and may result from nucleotides becoming

transiently available for modification during ‘breathing’, due to the dynamic nature of RNA structures.⁵⁵ The 5’ terminal two nucleotides (uridines at position 1 and 2) were highly reactive and therefore likely to be non-base paired.

3.2 | The effects of deletions to the distal or proximal regions of the S fragment stem-loop on replicon replication

The SHAPE data and the structural prediction described in Figure 1 were used to design a series of truncations to the S fragment, and the modified sequences were introduced into a replicon. The replicon was based on an infectious clone of FMDV O1K in which the P1 region of the genome is replaced with a ptGFP reporter³⁰ (Figure 2A). Deletions were designed to end at either the top or bottom of bulges, helping ensure that the stem-loop hairpin

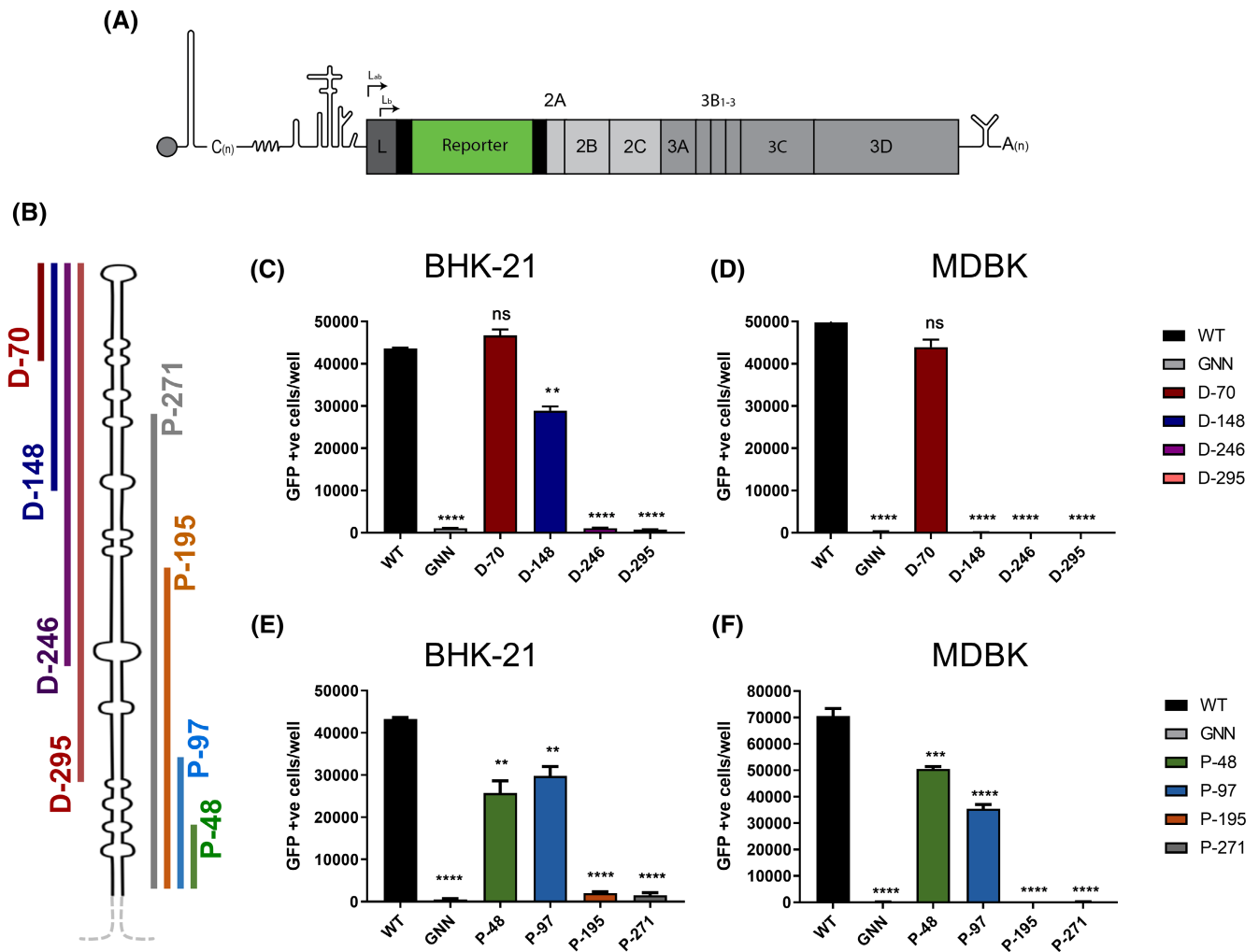


FIGURE 2 Truncations to the distal and proximal regions of the S fragment can impair replication. (A) Cartoon schematic of FMDV O1K replicon with the region encoding the structural proteins replaced with a GFP reporter. (B) Schematic representation of S fragment deletions. The maintained 3' and 5' proximal (P) regions are represented by the dotted gray line and was constant in all deletions. The colored lines indicate the part of the S fragment which was removed. (C,D) Replication of replicons with 70, 148, 246 and 295 nucleotides removed from the distal (D) region of the S fragment was measured following transfection into BHK-21 cells or MDBK cells. Replication was monitored by GFP expression using an IncuCyte, shown at 8 h post-transfection. The parental construct (which contains additional restriction sites to facilitate generation of the deletions) is included as a positive control and termed WT. Similarly, a 3D^{pol} inactive mutant 'GNN' (which includes the same restriction sites) is included as a control for input translation levels. (E,F) Replication of replicons with 48, 97, 195 and 271 nucleotides removed from the proximal (P) region of the S fragment and measured as in (C) ($n=3$, error bars represent SEM) ** $p < .01$, *** $p < .001$, **** $p < .0001$.

structure was maintained. To facilitate replacement of the S fragment with modified sequences *EagI* restriction sites were introduced at each end of the S fragment sequence. These sites required minimal modification of the original sequence and showed no predicted change in RNA structure, and the modified genome sequence is hereafter referred to as WT. Addition of the *EagI* site at the 5' end of the S fragment resulted in a large reduction in replication; however, when paired with the 3' *EagI* site, restoring base pairing, replicative potential was drastically improved, although still below that of the original O1K WT sequence (Figure S1). Deletions of 70, 148, 246 and 295 nucleotides

were introduced at the distal end (top) of the S fragment stem-loop (constructs named D-70, D-148, D-246 and D-295, respectively) and deletions of 48, 97, 195 and 271 nucleotides were made to the proximal end (bottom) of the S fragment (constructs referred to as P-48, P-97, P-195 and P-271, respectively) (Figure 2B). The truncated sequences were chemically synthesized and introduced into the WT replicon via the *EagI* sites, meaning that the highly conserved 5' and 3' regions and essential UU nucleotides at positions 1 and 2 were maintained in all truncation mutants. RNAs from the eight new replicon clones were transfected into BHK-21 or MDBK cells, alongside WT and a

3D^{pol}-GNN replication-negative control. For this control, the GFP signal produced represents translation of the input RNA only. BHK-21 and MDBK cells are continuous cell lines known to support replication of FMDV: BHK-21 cells are used for FMDV vaccine production, whereas MDBK cells originate from a natural host of FMDV. Replication was monitored by measuring reporter expression using an InCuCyte ZOOM live cell imaging system, with analysis by our established protocols (performed 8 h post transfection, when replication has reached its peak (Figure S2)) (Figure 2). As a control, we ensured that removal of the S fragment did not affect RNA stability (Figure S3).

As described previously and consistent with sequence information from natural virus isolates,^{8,26} the D-70 mutation caused no significant drop in replication in either cell line. However, the replicon bearing the D-148 deletion, which removes the distal half of the S fragment stem-loop, showed reduced replication in BHK-21 cells and none in MDBK cells (Figure 2C,D). Innate immunity is compromised in BHK-21 cells but intact in MDBK cells,^{56,57} suggesting that the distal portion of the S fragment stem-loop plays a role in modulating a competent host immune response, in agreement with previously published data.^{25,58} Replicons with the largest distal deletions, D-246 and D-295, did not replicate in either cell line.

While the consequences of deleting sequences from the distal region of the S fragment stem-loop have been reported,²⁵ the effects of proximal deletions have not been investigated. The two smallest proximal deletions (P-48 and P-97) showed modest but significant decreases in replication compared to WT (1.7 and 1.4-fold, respectively) (Figure 2E,F). However, the larger deletions, P-195 and P-271, completely ablated replication and reporter gene expression was reduced to a level comparable to the GNN control. Interestingly, there was no significant difference between the replication of the P-48 and P-97 deletions in either BHK-21 or MDBK cells (Figure 2). Overall, the proximal part of the S fragment stem-loop appears to be more sensitive to deletion in a cell type-independent manner, with truncations as small as 48 nucleotides having a significant effect on replication.

Earlier studies indicated that the proximal part of the S fragment stem-loop is more conserved than the distal part.⁸ In recent years, advances in high throughput sequencing (HTS) have led to a great increase in the number of FMDV full genome sequences available on public domains, including sequences of viruses of Southern African Territories (SAT) serotypes which were previously underrepresented. This increase in the range of sequences available prompted us to revisit the subject of the S fragment variability and we carried out a covariance analysis based on 118 FMDV isolates representing

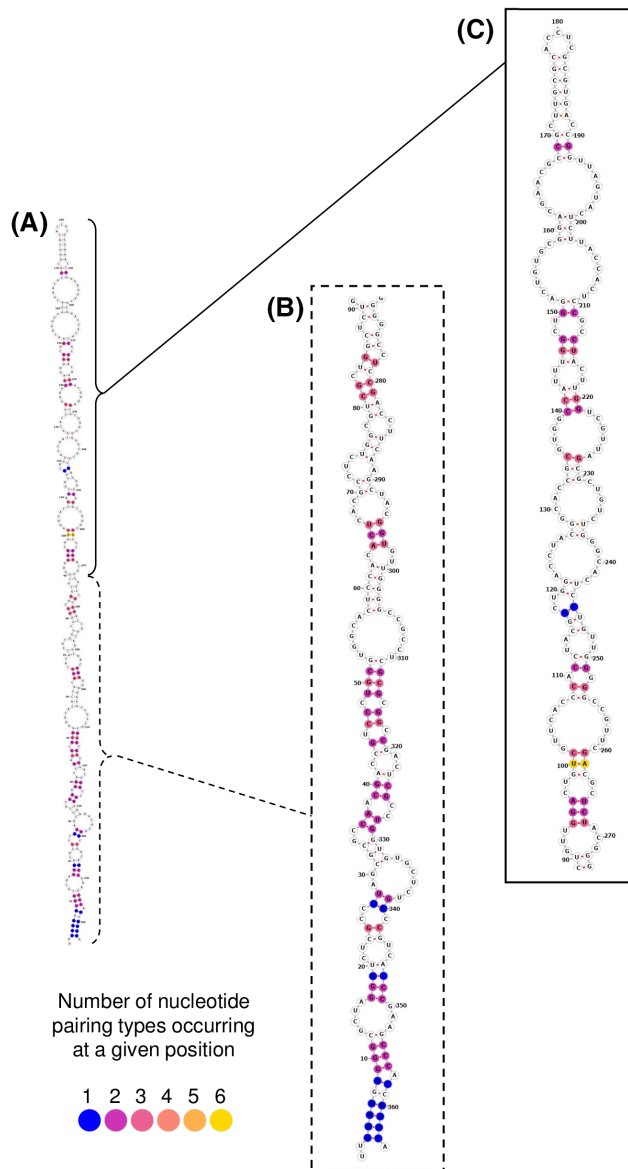


FIGURE 3 The extent of nucleotide and pairing conservation within the S fragment of the FMDV. (A) A schematic representation of conserved RNA structure of the S fragment in all 118 FMDV isolates. Nucleotide positions which form conserved pairing in 116/118 FMDV isolates were color-coded according to number of pairing types (purple for one nucleotide pairing type at a given position and yellow for six nucleotide pairing types; see the color matrix included at the bottom left corner of the figure). There are six possible nucleotide pairings: A-U, G-C, G-U, U-A, C-G and U-G. Nucleotide pairings which were not conserved in three or more FMDV isolates, remained white. Due to the length of the S fragment stem-loop, the resolution of the image was not sufficient for detailed view of the individual nucleotide pairings and so the S fragment was artificially divided into two parts, proximal and distal, and the images of their schematic RNA structures enlarged (B,C). (B) The proximal part of the S fragment included nucleotide positions 1–90 and 272–364, (C) while the distal part included nucleotide positions 90–272. Numbers represent nucleotide positions of the S fragment sequence.

all seven serotypes. Figure 3 shows that there is more base-pairing conservation in the proximal than in the distal parts of the S fragment stem-loop (Figure 3). The base-pairing conservation in the proximal part of the otherwise very variable S fragment stem-loop (low nucleotide identity of approximately 47%) suggests evolutionary pressure to maintain the structure of this portion of the stem-loop and complements our observations from the replicon experiments (Figure 2).^{8,10}

3.3 | Viruses with proximal deletions of the S fragment replicate more slowly than WT and can select for a mutation in 3D^{pol} during serial passage

We investigated the consequences of proximal deletions to the S fragment stem-loop further by introducing these truncations into an FMDV O1K infectious clone. This enabled evaluation of replication in the context of the entire genome and investigation of the possible selection of compensatory or adaptive mutations during serial passage. Replicons bearing proximal deletions of the S fragment stem-loop were converted into infectious clones by replacing the ptGFP reporter sequence with the original O1K structural protein sequence. RNA transcripts of the truncated S fragment clones and WT were transfected into BHK-21 cells. Supernatants containing recovered virus were harvested and used to infect naïve BHK-21 cells for 5 continuous passages. Recovery of infectious virus from each construct was assessed by the ability of 5th passage samples to induce CPE. As expected, CPE was induced and virus recovered from the WT construct. Infectious virus was also recovered from P-48 and P-97 but no virus was recovered from either P-195 or P-271 constructs (Table S3).

The consequences of the P-48 and P-97S fragment deletions for the dynamics of virus replication were investigated by assessing the time taken to induce CPE in BHK-21 cell monolayers after infection with the mutated viruses or WT at a low MOI of 0.01 PFU. The integrity of the cell monolayers was assessed at hourly intervals over 63h using live cell imaging monitored by IncuCyte S3 (Figure 4A). Both P-48 and P-97 viruses developed CPE more slowly than WT, as anticipated from the earlier replicon experiments (Figure 4A). For comparison, while a D-148 virus bearing a larger deletion from the distal end of the S fragment stem-loop replicated at a slower rate than the WT virus, D-148 replicated significantly faster than viruses carrying deletions at the proximal end of the S fragment (i.e., P-48 and P-97; Figure 4A); further confirming replicon experiments. Ability of the viruses to form plaques was also assessed. Both, P-48 and P-97 mutants

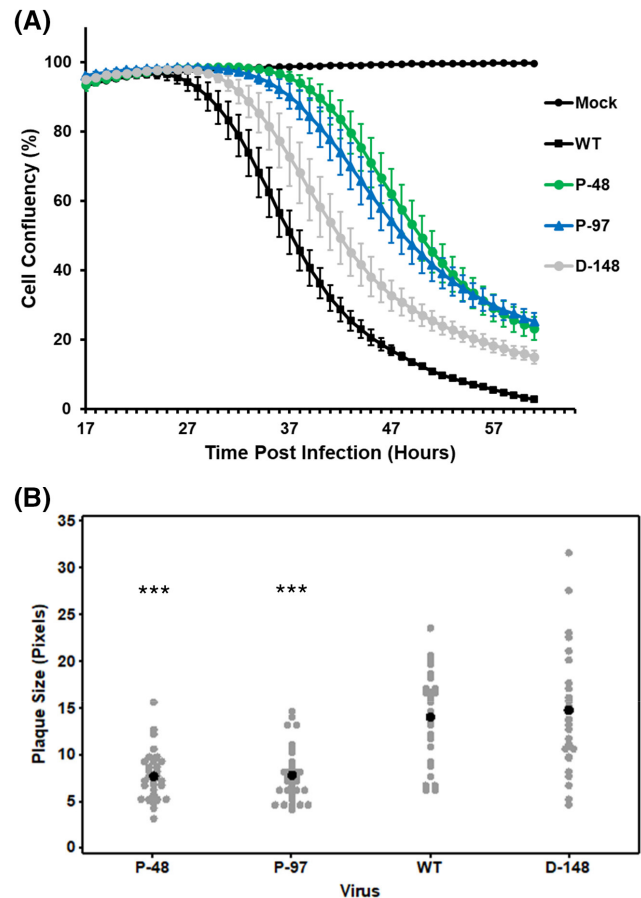


FIGURE 4 Fitness of FMDV containing a truncation at the proximal end of the S fragment. (A) Recovered WT, P-48, P-97 and D-148 virus populations were used to infect BHK-21 cells at an MOI of 0.01 PFU. CPE was monitored over time using an IncuCyte S3 live cell imaging and is shown as a reduction in cell confluency; ($n = 3$ error bars represent SEM). (B) Plaque sizes of the WT, P-48, P-97 and D-148 variants grown on BHK-21 cells. Each well containing plaques was scanned and the plaque size was estimated in pixels. All plaques were counted to avoid bias in plaque selection. Gray dots represent individual plaques, while black dot represents the mean; *** $p < .001$ when comparing to plaque size induced by the WT. Note that WT refers to the construct which contains additional restriction sites to facilitate generation of the deletions.

generated significantly smaller plaques when comparing to WT and/or D-148 mutant virus (Figure 4B).

Sequencing of recovered viruses revealed one isolate with mutations in the genomic region encoding the 2C protein, which were not investigated further. In addition, a single mutation in the 3D^{pol} sequence was found in a high proportion of the viral progeny of one of three P-97 viral replicates. The A7203C change resulted in I189L mutation in the 3D^{pol} protein amino acid sequence. The evolution of this mutation was investigated further by sequencing viruses from earlier passages. The proportion of the I189L mutation in the population increased from 40%

at passage 3 to 51% at passage 4, and 61% at passage 5, suggesting that this confers a selective advantage in the context of the proximal S fragment stem-loop deletion and so is sequentially enriched. With four exceptions out of 1123 sequences of 3D^{pol} available, all known FMDV isolates have isoleucine at this position (Figure S4), making the amino acid substitution for leucine novel. This residue is known to interact with template RNA (Figure 5A),

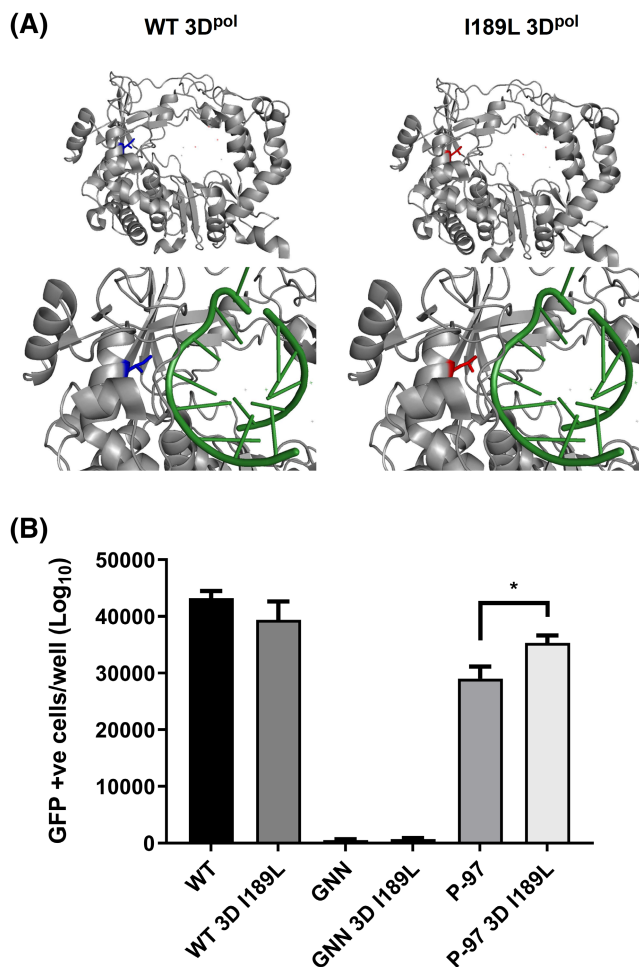


FIGURE 5 Compensatory mutation I189L in the structure of 3D^{pol} and its effect on replication of FMDV replicons. (A) WT 3D^{pol} crystal structure with I189 residue highlighted in blue, shown with (bottom, left) and without bound RNA (top, left). The I189L residue mutation was modeled onto the WT 3D^{pol} crystal structure and highlighted in red (right). Structure shown with (bottom, right) and without (top, right) bound RNA. The PDB file used was 1WNE. (B) The 3D^{pol} I189L mutation was introduced into WT, GNN and P-97 replicons, termed WT I189L, GNN I189L and P-97 I189L, respectively. Replicon RNA was transcribed and transfected into BHK-21 cells. WT and 3D^{pol} GNN replicons were included as controls, with the latter for the level of input translation ($n = 3$ error bars represent SEM, $*p < .05$). The WT and GNN constructs also included additional restriction sites to facilitate generation of the deletions.

playing a crucial role during viral replication.³² No such mutations were observed in the WT or the P-48 mutant viruses after passage.

3.4 | Effect of the 3D^{pol} I189L compensatory mutation on replicon replication

Considering the importance and conserved nature of the 3D^{pol} I189 residue in wild-type viruses, we investigated whether the 3D^{pol} I189L mutation compensates for the loss of fitness of P-97, the replicon bearing the largest viable proximal truncation to the S fragment. This would suggest an interaction between the proximal part of the S fragment and the viral polymerase. To test this, the I189L mutation was introduced into WT, GNN and P-97 replicons by site-specific mutagenesis and the consequence for replication (assessed by reporter gene expression following transfection into BHK-21 cells) was investigated as above. Introduction of 3D^{pol} I189L into the WT replicon had no significant effect on replication, however, a small but significant increase in replication was observed when it was introduced into the P-97 replicon (Figure 5B). As expected, I189L was unable to restore the activity of the GNN negative control.

3.5 | I189L modifies 3D^{pol} activity

The influence of the 3D^{pol} I189L mutation on polymerase function was investigated using Sym/Sub assay; a highly sensitive method for interrogating polymerase activity. Sym/Sub assays have been used to study PV replication and enable extension of a radiolabelled template to be measured at the single nucleotide level.⁴⁸ The method uses a 10-nucleotide template oligonucleotide which base-pairs to create a small double stranded region with a four nucleotide 5' overhang, thus allowing 3' nucleotide addition. In the presence of rNTPs and recombinantly expressed 3D^{pol}, the addition of single or multiple nucleotides can be assessed over time by separating input template and elongation products by gel electrophoresis (Figure 6A). Initially, an assay using ATP only was undertaken to probe the ability of the enzyme to add a single nucleotide. WT and I189L 3D^{pol} proteins behaved similarly in the assay with no differences in the rate of addition of the single nucleotide (Figure 6B,C).

3D^{pol} activity was examined further by including all four rNTPs into the Sym/Sub assay. The design of the Sym/Sub oligonucleotide allows for elongation by a maximum of +4 nucleotides to produce a fully double stranded

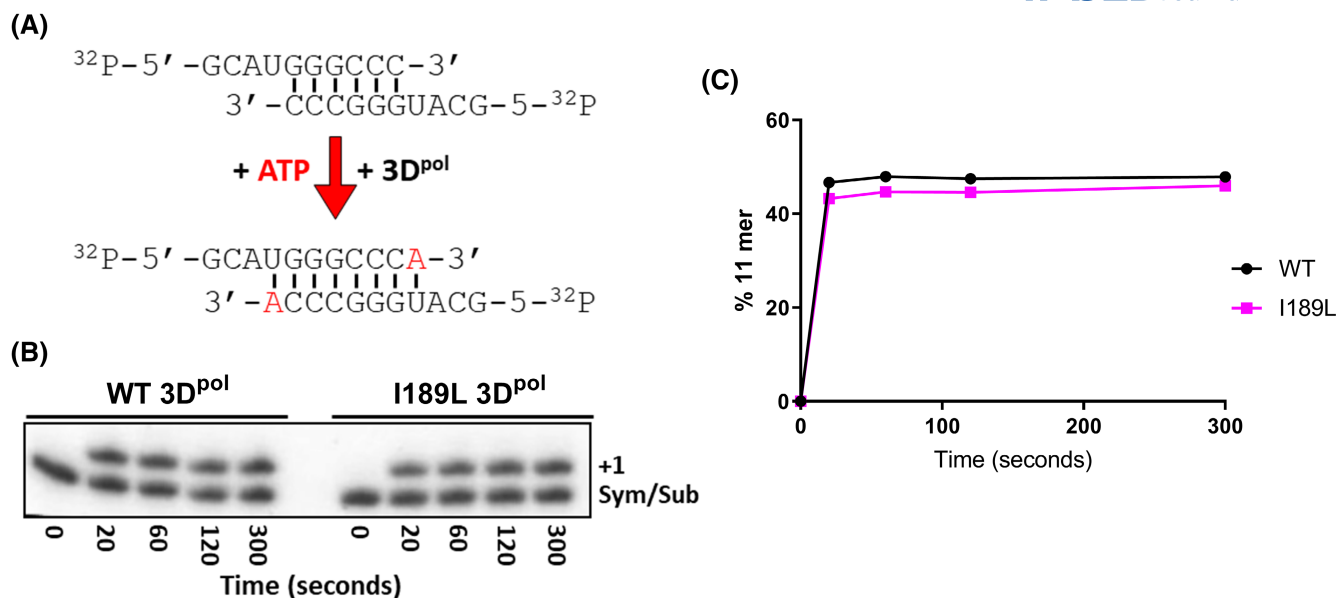


FIGURE 6 Single nucleotide addition to a Sym/Sub substrate by WT and I189L 3D^{pol}. (A) Schematic of the Sym/Sub experimental protocol. Radioactively end labeled RNA oligonucleotides are annealed before addition of rNTPs and recombinant 3D^{pol}. (B) Extension of the 10mer Sym/Sub template with a single nucleotide (ATP) using either WT or I189L FMDV 3D^{pol}. Aliquots of the reactions were taken at 20, 60, 120 and 300 s, RNA fragments separated by electrophoresis and visualized using a phosphorimager. (C) Densitometry of +1 product is plotted as rate of addition of a single nucleotide shown over time, % +1 product refers to the total amount of input Sym/Sub template that was extended by 1 nucleotide.

product (Figure 7A). Both the WT and the I189L 3D^{pol} enzymes produced the expected +4 product. In addition, a longer product equivalent to +12 nucleotides was produced by both polymerases (as calculated by Rf value for migration traveled) (Figure 7B). This is reminiscent of the larger products seen in recombination assays reported in the investigation of PV 3D^{pol}.^{48,59} Although there was no measurable difference in rate of addition of the four nucleotides by WT or mutant enzyme, I189L 3D^{pol} produced more of the larger +12 product (Figure 7C,D). The enhanced generation of this product shows that the I189L mutation altered the activity of 3D^{pol} in vitro and also resulted in improved replication of the P-97 replicon (Figure 5B). These results suggest that I189L is a compensatory mutation conferring a replicative advantage to the replicon carrying the largest viable proximal truncation of the S fragment stem-loop and implies that the 3D^{pol} and the S fragment interact during replication of FMDV.

4 | DISCUSSION

In comparison to other picornaviruses, the 5' UTR of FMDV is uniquely large and complex, comprising several distinct structural domains, the functions of most of which are poorly understood. The first *c.* 360 nucleotides are predicted to form a single, long stem-loop called the S fragment.²⁴ Although supported by functional studies, to

our knowledge the secondary structure of the S fragment has not been determined biochemically.²⁵ Here, using SHAPE chemistry applied to a sequence of a well-studied FMDV isolate (O1 Kaufbeuren),³³ we confirm that the S fragment folds into a single, long stem-loop containing several bulges formed by unpaired nucleotides. The importance of some of these bulges for viral viability was determined previously.²⁵

We show that although deletion of 246 nucleotides or more from the distal region on the S fragment was not tolerated, mutants carrying deletions D-70 and D-148 remained replication-competent. Despite the high sequence and length variability of the S fragment observed in FMDV field isolates, most viruses maintain the full-length stem-loop.¹⁰ This suggests a strong evolutionary pressure to maintain the structure. The S fragment is known to interact with viral and cellular proteins and the 3' UTR, likely facilitating circularization of the viral genome during replication.⁶⁰⁻⁶² However, there is evidence that some deletions to the distal part of the S fragment are tolerated and a number of unrelated field isolates from different FMDV serotypes (e.g., A, C and O) have been shown to carry deletions in S fragments. These deletions arose independently and range in length from few to 76 nucleotides.^{8,26,63} Unlike deletions found in other parts of the FMDV genome (e.g. deletions found in the region encoding 3A), those found in the S fragment do not appear to be host specific, with viruses carrying deletions within the

sugar-phosphate backbone of the template RNA during viral replication.³² Given the essential role of I189 in viral RNA replication, we investigated the effect of the I189L mutation on replication and RNA strand synthesis. Introduction of I189L into the P-97 replicon enhanced replication, suggesting an advantageous effect of this mutation. Biochemical analysis of the I189L 3D^{pol} mutant did not indicate an altered rate of nucleotide incorporation when compared to the WT polymerase. However, the synthesis of a larger than predicted +12 product was greater with the I189L 3D^{pol} enzyme compared to WT. This suggests that the I189L mutation may influence the fidelity of the polymerase, possibly due to an altered interaction between the amino acid side chain and the RNA template. Extended products have been observed in similar reactions with the 3D^{pol} of PV and were proposed to be the result of a nucleotide misincorporation, facilitating a template switch.^{48,59,64} In addition, it has been reported that greater fidelity of viral RNA polymerases is associated with increased insertion/deletion (indel) events during viral replication.⁵⁹ Whether the longer product observed here occurred as the result of strand slippage, or a template switch remains to be investigated. Nevertheless, slow accumulation of the compensatory mutation over serial passage in a virus carrying maximal viable proximal deletion to the S fragment structure, and the small advantageous effect of this mutation on replicon replication suggests the possibility of (direct or indirect) interaction between the S fragment and the viral polymerase (or its precursor). Further studies are required to verify this interplay.

In conclusion, using biochemical methods, we confirmed a previously proposed secondary structure of the S fragment of FMDV. Despite its higher sequence and nucleotide pairing conservation, small deletions to the proximal part of the S fragment stem-loop are viable, although resulting in attenuated replicons and viruses. An advantageous compensatory mutation within a highly conserved site of 3D^{pol} appeared during serial passage of a viral isolate bearing the largest viable mutation to the proximal part of the S fragment, suggesting potential interactions between the S fragment and the viral polymerase during replication.

AUTHOR CONTRIBUTIONS

J. C. Ward, L. Lasecka-Dykes, S. J. Dobson, S. Gold, N. J. Kingston, M. R. Herod performed research. D. P. King, T. J. Tuthill, D. J. Rowlands M. R. Herod and N. J. Stonehouse provided supervision, data interpretation and project funding. The research was designed by D. J. Rowlands, M. R. Herod and N. J. Stonehouse. All authors contributed to the writing of the manuscript, with J. C. Ward, L. Lasecka-Dykes taking the lead in writing and data analysis. J. C. Ward, L. Lasecka-Dykes should be considered joint first

authors and D. J. Rowlands and N. J. Stonehouse as joint senior authors.

ACKNOWLEDGMENTS

None.

FUNDING INFORMATION

This work was supported by the Biotechnology and Biological Sciences Research Council (BBSRC) of the United Kingdom (research grant BB/K003801/1). Additionally, The Pirbright Institute receives grant-aided support from the BBSRC (projects BBS/E/I/00007035, BBS/E/I/00007036 and BBS/E/I/00007037) and the UK Department for the Environment, Food and Rural Affairs (Defra project SE2945).

DISCLOSURES

The authors have stated explicitly that there are no conflicts of interest in connection with this article.

DATA AVAILABILITY STATEMENT

Additional information and data underpinning the work described here (e.g. primer sequences) can be obtained by contacting the corresponding authors.

ORCID

Joseph C. Ward  <https://orcid.org/0000-0001-9867-393X>

Lidia Lasecka-Dykes  <https://orcid.org/0000-0003-3188-4198>

Samuel J. Dobson  <https://orcid.org/0000-0002-8815-7381>

Sarah Gold  <https://orcid.org/0000-0003-0501-9707>

Natalie J. Kingston  <https://orcid.org/0000-0001-7109-6757>

Morgan R. Herod  <https://orcid.org/0000-0002-8626-6787>

Donald P. King  <https://orcid.org/0000-0002-6959-2708>

Tobias J. Tuthill  <https://orcid.org/0000-0002-6582-388X>

David J. Rowlands  <https://orcid.org/0000-0002-4742-9272>

Nicola J. Stonehouse  <https://orcid.org/0000-0003-1146-5519>

<https://orcid.org/0000-0002-8626-6787>

<https://orcid.org/0000-0002-6959-2708>

<https://orcid.org/0000-0002-6582-388X>

<https://orcid.org/0000-0002-4742-9272>

<https://orcid.org/0000-0003-1146-5519>

<https://orcid.org/0000-0002-8626-6787>

REFERENCES

1. Lulla V, Dinan AM, Hosmillo M, et al. An upstream protein-coding region in enteroviruses modulates virus infection in gut epithelial cells. *Nat Microbiol.* 2019;4:280-292.
2. Roos RP, Kong W-P, Semler BL. Polyprotein processing of Theiler's murine encephalomyelitis virus. *J Virol.* 1989;63:5344-5353.
3. Martínez-Salas E, Francisco-Velilla R, Fernandez-Chamorro J, Lozano G, Diaz-Toledano R. Picornavirus IRES elements: RNA structure and host protein interactions. *Virus Res.* 2015;206:62-73.

4. Mason PW, Bezborodova SV, Henry TM. Identification and characterization of a cis-acting replication element (cre) adjacent to the internal ribosome entry site of foot-and-mouth disease virus. *J Virol.* 2002;76:9686-9694.
5. Goodfellow IG, Kerrigan D, Evans DJ. Structure and function analysis of the poliovirus cis-acting replication element (CRE). *RNA.* 2003;9:124-137.
6. Goodfellow I, Chaudhry Y, Richardson A, et al. Identification of a cis-acting replication element within the poliovirus coding region. *J Virol.* 2000;74:4590-4600.
7. Barton DJ, O'Donnell BJ, Flanagan JB. 5' cloverleaf in poliovirus RNA is a cis-acting replication element required for negative-strand synthesis. *EMBO J.* 2001;20:1439-1448.
8. Carrillo C, Tulman ER, Delhon G, et al. Comparative genomics of foot-and-mouth disease virus. *J Virol.* 2005;79:6487-6504.
9. Ward JC, Lasecka-Dykes L, Neil C, et al. The RNA pseudoknots in foot-and-mouth disease virus are dispensable for genome replication, but essential for the production of infectious virus. *PLoS Pathog.* 2022;18:e1010589.
10. Lasecka-Dykes L, Wright CF, Di Nardo A, et al. Full genome sequencing reveals new southern African territories genotypes bringing us closer to understanding true variability of foot-and-mouth disease virus in Africa. *Viruses.* 2018;10:192.
11. Lopez de Quinto S. IRES-driven translation is stimulated separately by the FMDV 3'-NCR and poly(a) sequences. *Nucleic Acids Res.* 2002;30:4398-4405.
12. Chard LS, Kaku Y, Jones B, Nayak A, Belsham GJ. Functional analyses of RNA structures shared between the internal ribosome entry sites of hepatitis C virus and the picornavirus porcine teschovirus 1 Talfan. *J Virol.* 2006;80:1271-1279.
13. Carocci M, Bakkali-Kassimi L. The encephalomyocarditis virus. *Virulence.* 2012;3:351-367.
14. Drexler JF, Corman VM, Lukashev AN, et al. Evolutionary origins of hepatitis a virus in small mammals. *Proc Natl Acad Sci USA.* 2015;112:15190-15195.
15. Knight-Jones TJD, Rushton J. The economic impacts of foot and mouth disease – what are they, how big are they and where do they occur? *Prev Vet Med.* 2013;112:161-173.
16. Mahapatra M, Parida S. Foot and mouth disease vaccine strain selection: current approaches and future perspectives. *Expert Rev Vaccines.* 2018;17:577-591.
17. Park J-H. Requirements for improved vaccines against foot-and-mouth disease epidemics. *Clin Exp Vaccine Res.* 2013;2:8-18.
18. Stenfeldt C, Eschbaumer M, Rekant SI, et al. The foot-and-mouth disease carrier state divergence in cattle. *J Virol.* 2016;90:6344-6364.
19. Sweeney TR, Cisnetto V, Bose D, et al. Foot-and-mouth disease virus 2C is a hexameric AAA+ protein with a coordinated ATP hydrolysis mechanism. *J Biol Chem.* 2010;285:24347-24359.
20. Teterina NL, Gorbalenya AE, Egger D, Bienz K, Rinaudo MS, Ehrenfeld E. Testing the modularity of the N-terminal amphipathic helix conserved in picornavirus 2C proteins and hepatitis C NS5A protein. *Virology.* 2006;344:453-467.
21. Bienz K, Egger D, Troxler M, Pasamontes L. Structural organization of poliovirus RNA replication is mediated by viral proteins of the P2 genomic region. *J Virol.* 1990;64:1156-1163.
22. Black DN, Stephenson P, Rowlands DJ, Brown F. Sequence and location of the poly C tract in aphtho- and cardiocivirus RNA. *Nucleic Acids Res.* 1979;6:2381-2390.
23. Mellor EJC, Brown F, Harris TJR. Analysis of the secondary structure of the poly(C) tract in foot-and-mouth disease virus RNAs. *J Gen Virol.* 1985;66:1919-1929.
24. Clarke BE, Brown AL, Currey KM, Newton SE, Rowlands DJ, Carroll AR. Potential secondary and tertiary structure in the genomic RNA of foot and mouth disease virus. *Nucleic Acids Res.* 1987;15:7067-7079.
25. Kloc A, Diaz-San Segundo F, Schafer EA, et al. Foot-and-mouth disease virus 5'-terminal S fragment is required for replication and modulation of the innate immune response in host cells. *Virology.* 2017;512:132-143.
26. Valdazo-González B, Timina A, Scherbakov A, Abdul-Hamid N, Knowles NJ, King DP. Multiple introductions of serotype O foot-and-mouth disease viruses into East Asia in 2010–2011. *Vet Res.* 2013;44:76.
27. Xiang W, Harris K, Alexander L, Wimmer E. Interaction between the 5'-terminal cloverleaf and 3AB/3CDpro of poliovirus is essential for RNA replication. *J Virol.* 1995;69:3658-3667.
28. Serrano P, Pulido MR, Sáiz M, Martínez-Salas E. The 3' end of the foot-and-mouth disease virus genome establishes two distinct long-range RNA-RNA interactions with the 5' end region. *J Gen Virol.* 2006;87:3013-3022.
29. Forrest S, Lear Z, Herod MR, Ryan M, Rowlands DJ, Stonehouse NJ. Inhibition of the foot-and-mouth disease virus subgenomic replicon by RNA aptamers. *J Gen Virol.* 2014;95:2649-2657.
30. Tulloch F, Pathania U, Luke GA, et al. FMDV replicons encoding green fluorescent protein are replication competent. *J Virol Methods.* 2014;209C:35-40.
31. Herod MR, Ferrer-Orta C, Loundras E-A, et al. Both cis and trans activities of foot-and-mouth disease virus 3D polymerase are essential for viral RNA replication. *J Virol.* 2016;90:6864-6883.
32. Ferrer-Orta C, Arias A, Perez-Luque R, Escarmis C, Domingo E, Verdager N. Structure of foot-and-mouth disease virus RNA-dependent RNA polymerase and its complex with a template-primer RNA. *J Biol Chem.* 2004;279:47212-47221.
33. Bentham M, Holmes K, Forrest S, Rowlands DJ, Stonehouse NJ. Formation of higher-order foot-and-mouth disease virus 3Dpol complexes is dependent on elongation activity. *J Virol.* 2012;86:2371-2374.
34. Herod MR, Tulloch F, Loundras E-A, Ward JC, Rowlands DJ, Stonehouse NJ. Employing transposon mutagenesis to investigate foot-and-mouth disease virus replication. *J Gen Virol.* 2015;96:3507-3518.
35. Herod MR, Gold S, LaseckaDykes L, et al. Genetic economy in picornaviruses: foot-and-mouth disease virus replication exploits alternative precursor cleavage pathway. *PLoS Pathog.* 2017;13:e1006666.
36. Lorenz R, Bernhart SH, Höner zu Siederdisen C, et al. ViennaRNA package 2.0. *Algorithms Mol Biol.* 2011;6:1-14.
37. King AMQ, Blakemore WE, Ellard FM, Drew J, Stuart DI. Evidence for the role of His-142 of protein 1C in the acid-induced disassembly of foot-and-mouth disease virus capsids. *J Gen Virol.* 1999;80:1911-1918.
38. Logan G, Freimanis GL, King DJ, et al. A universal protocol to generate consensus level genome sequences for foot-and-mouth disease virus and other positive-sense polyadenylated RNA viruses using the Illumina MiSeq. *BMC Genomics.* 2014;15:828.
39. Acevedo A, Andino R. Library preparation for highly accurate population sequencing of RNA viruses. *Nat Protoc.* 2014;9:1760-1769.

40. GitHub. najoshi/sickle: Windowed Adaptive Trimming for fastq files using quality.
41. Peng Y, Leung HCM, Yiu SM, Chin FYL. IDBA-UD: a de novo assembler for single-cell and metagenomic sequencing data with highly uneven depth. *Bioinformatics*. 2012;28:1420-1428.
42. Altschul SF, Gish W, Miller W, Myers EW, Lipman DJ. Basic local alignment search tool. *J Mol Biol*. 1990;215:403-410.
43. Li H, Durbin R. Fast and accurate long-read alignment with Burrows–Wheeler transform. *Bioinformatics*. 2010;26:589-595.
44. Robinson JT, Thorvaldsdóttir H, Winckler W, et al. Integrative genomics viewer. *Nat Biotechnol*. 2011;29:24-26.
45. Li H, Durbin R. Fast and accurate short read alignment with Burrows–Wheeler transform. *Bioinformatics*. 2009;25:1754-1760.
46. Li H. Aligning Sequence Reads, Clone Sequences and Assembly Contigs with BWA-MEM. 2013.
47. Jackson T, Sheppard D, Denyer M, Blakemore W, King AMQ. The epithelial integrin $\alpha\beta 6$ is a receptor for foot-and-mouth disease virus. *J Virol*. 2000;74:4949.
48. Arnold JJ, Cameron CE. Poliovirus RNA-dependent RNA polymerase (3D(pol)). Assembly of stable, elongation-competent complexes by using a symmetrical primer-template substrate (sym/sub). *J Biol Chem*. 2000;275:5329-5336.
49. de la Higuera I, Ferrer-Orta C, Moreno E, et al. Contribution of a multifunctional polymerase region of foot-and-mouth disease virus to lethal mutagenesis. *J Virol*. 2018;92:e01119-18.
50. Wright CF, Knowles NJ, Di Nardo A, Paton DJ, Haydon DT, King DP. Reconstructing the origin and transmission dynamics of the 1967–68 foot-and-mouth disease epidemic in the United Kingdom. *Infect Genet Evol*. 2013;20:230-238.
51. Lasecka-Dykes L, Tulloch F, Simmonds P, et al. Mutagenesis mapping of RNA structures within the foot-and-mouth disease virus genome reveals functional elements localized in the polymerase (3Dpol)-encoding region. *mSphere*. 2021;6:e0001521.
52. Kerpedjiev P, Hammer S, Hofacker IL. Forna (force-directed RNA): simple and effective online RNA secondary structure diagrams. *Bioinformatics*. 2015;31:3377-3379.
53. Schneider TD, Stephens RM. Sequence logos: a new way to display consensus sequences. *Nucleic Acids Res*. 1990;18:6097.
54. Crooks GE, Hon G, Chandonia JM, Brenner SE. WebLogo: a sequence logo generator. *Genome Res*. 2004;14:1188-1190.
55. Homan PJ, Favorov OV, Lavender CA, et al. Single-molecule correlated chemical probing of RNA. *Proc Natl Acad Sci USA*. 2014;111:13858-13863.
56. Conzelmann KK. Reverse genetics of Mononegavirales. *Curr Top Microbiol Immunol*. 2004;283:1-41.
57. Schlender J, Bossert B, Buchholz U, Conzelmann K-K. Bovine respiratory syncytial virus nonstructural proteins NS1 and NS2 cooperatively antagonize alpha/Beta interferon-induced antiviral response. *J Virol*. 2000;74:8234-8242.
58. Luna VER, Luk ADH, Tying SK, Hellman JM, Lefkowitz SS. Properties of bovine interferons. *Experientia*. 1984;40(12):1410-1412.
59. Woodman A, Arnold JJ, Cameron CE, Evans DJ. Biochemical and genetic analysis of the role of the viral polymerase in enterovirus recombination. *Nucleic Acids Res*. 2016;44:6883-6895.
60. Lawrence P, Rieder E. Identification of RNA helicase A as a new host factor in the replication cycle of foot-and-mouth disease virus. *J Virol*. 2009;83:11356-11366.
61. Rodríguez-Pulido M, Borrego B, Sobrino F, Sáiz M. RNA structural domains in noncoding regions of the foot-and-mouth disease virus genome trigger innate immunity in porcine cells and mice. *J Virol*. 2011;85:6492.
62. Rodríguez Pulido M, Serrano P, Sáiz M, Martínez-Salas E. Foot-and-mouth disease virus infection induces proteolytic cleavage of PTB, eIF3a,b, and PABP RNA-binding proteins. *Virology*. 2007;364:466-474.
63. Mohapatra JK, Pawar SS, Tosh C, et al. Genetic characterization of vaccine and field strains of serotype a foot-and-mouth disease virus from India. *Acta Virol*. 2011;55:349-352.
64. Arnold JJ, Cameron CE. Poliovirus RNA-dependent RNA polymerase (3D(pol)) is sufficient for template switching in vitro. *J Biol Chem*. 1999;274:2706-2716.

SUPPORTING INFORMATION

Additional supporting information can be found online in the Supporting Information section at the end of this article.

How to cite this article: Ward JC, Lasecka-Dykes L, Dobson SJ, et al. The dual role of a highly structured RNA (the S fragment) in the replication of foot-and-mouth disease virus. *The FASEB Journal*. 2024;38:e23822. doi:[10.1096/fj.202400500R](https://doi.org/10.1096/fj.202400500R)